Effect of off-stoichiometry and site disorder on the properties of Ni_3Al: I. Electrical and magneto-transport

2008 J. Phys.: Condens. Matter 20 445227

(http://iopscience.iop.org/0953-8984/20/44/445227)

J. Phys.: Condens. Matter **20** (2008) 445227 (15pp) doi:10.1088/0953-8984/20/44/445227

Effect of off-stoichiometry and site disorder on the properties of Ni_3Al: I. Electrical and magneto-transport

A C Abhyankar and S N Kaul[1]

School of Physics, University of Hyderabad, Central University PO, Hyderabad 500046, Andhra Pradesh, India

E-mail: kaul.sn@gmail.com

Received 1 April 2008, in final form 2 August 2008
Published 10 October 2008
Online at stacks.iop.org/JPhysCM/20/445227

Abstract

Electrical resistivity, $\rho(T)$, and longitudinal magnetoresistance, $\Delta\rho_{\parallel}/\rho = [\rho_{\parallel}(T, H) - \rho(T, H = 0)]/\rho(T, H = 0)$, of 'as-prepared' Ni_xAl_{100-x} alloys with $x = 74.3$, 74.8, 75.1 and 76.1 at.% and 'annealed' $Ni_{75.1}Al_{24.9}$ alloy, measured over wide ranges of temperature and external magnetic field (H), are discussed in the light of existing theoretical models. $\rho(T)$ exhibits a non-Fermi liquid (NFL) behaviour at low temperatures in the range 1.7 K $\leqslant T \leqslant T_x$ (where T_x decreases from 25 to 21 K as the Ni concentration x increases from 74.3 to 75.1 at.%) in the alloys with $x < 76.1$ at.%. Compositional disorder (particularly under-stoichiometry) gives rise to stronger deviations from the Fermi liquid behaviour and widens the temperature range over which the NFL behaviour persists whereas *site disorder* makes the NFL behaviour more prominent, particularly in the stoichiometric composition (Ni_3Al), and stabilizes the NFL behaviour in any given composition over a much wider temperature range. The main contributions to $\rho(T)$ and $\Delta\rho_{\parallel}/\rho$ arise from the scattering of conduction electrons from the 'unconventional' spin waves (exchange-enhanced non-propagating spin-density fluctuations) at low temperatures (intermediate temperatures and temperatures close to the Curie point, T_C). The self-consistent spin fluctuation theory correctly predicts that H leaves the functional dependence of ρ on temperature unaltered and quantitatively describes the suppression of the spin-wave and spin-density fluctuation contributions to ρ by H in different temperature regimes.

1. Introduction

Substantial progress has been made in understanding electrical and thermal transport in nearly ferromagnetic (NF) and weakly ferromagnetic (WF) metals since Mills and Lederer [1] calculated electrical resistivity at low temperatures due to spin waves (SW) using the random phase approximation (RPA) within the framework of a simple model in which the conduction electrons (s-electrons) are scattered by the spin fluctuations (SF) of the d-band electrons via s–d exchange interaction. Subsequently, Schindler and Rice [2] (Mathon [3]) applied this model to NF (both NF and WF) metals to investigate electrical and thermal resistivity (electrical resistivity) at low temperatures near the critical boundary, which separates the nearly and weakly ferromagnetic regimes, by employing the RPA for calculating the dynamical susceptibility due to spin fluctuations. Schindler and Rice [2] found that electrical resistivity ($\rho(T)$) varies with temperature as T^2 at low temperatures, and as the critical boundary is approached from the NF side, the coefficient of the T^2 term becomes large while the temperature range over which $\rho(T)$ follows this power law behaviour narrows down. In contrast, Mathon [3] obtained the result that $\rho_{SF}(T) \sim T^{5/3}$ at very low temperatures on either side, but in the immediate vicinity, of the critical boundary. However, it was soon realized that the RPA does not yield the correct results, particularly at high temperatures where the interactions between different spin fluctuation modes become important. Ueda and Moriya [4] (UM), thus, used the self-consistently renormalized (SCR) spin fluctuation theory [5] (which provides a correct description for

[1] Author to whom any correspondence should be addressed.

the main attributes of weak itinerant-electron ferromagnets, including the Curie–Weiss behaviour of susceptibility for temperatures above the Curie temperature, T_C), instead of the RPA, to calculate the dynamical susceptibility and thereby the SF (SW) contributions to the electrical and thermal resistivity in NF and WF (WF) metals over an extremely wide temperature range. In summary, their results pertaining to resistivity are: (i) at very low temperatures, $\rho_{SW}(T) \sim T^2$ ($\rho_{SF}(T) \sim T^2$) for WF metals (on both sides of the critical boundary, where the ferromagnetic instability sets in), (ii) as the critical boundary is approached either from the nearly ferromagnetic side or from the weakly ferromagnetic side, the coefficient of the T^2 term in $\rho_{SF}(T)$ increases steeply while the temperature range over which this power law holds becomes narrow and (iii) a crossover from the T^2 variation to the $T^{5/3}$ variation occurs as the temperature is raised from low temperatures in NF metals whereas $\rho_{SF}(T) \sim T^{5/3}$ at temperatures close to T_C and $\rho_{SF}(T) \sim T$ at $T \gg T_C$ in WF metals. Ueda [6] extended the UM formalism [4, 5] to ascertain the effect of external magnetic field (H) on the SF contribution to $\rho(T)$ at low temperatures in weak itinerant-electron ferromagnets but neglected the SW contribution. Pai and Mishra [7] were the first to investigate the influence of disorder (caused by either impurities or off-stoichiometry or both) on electrical and thermal conductivity of NF metals at very low temperatures using the Keldysh diagram technique. Recently, the self-consistent calculations, due to Kaul [8], of the SW and SF contributions to $\rho(T)$ of weak itinerant-electron ferromagnets in the absence and presence of H at temperatures up to T_C overcame the main weakness of the UM [4, 5] and Ueda [6] theoretical treatments by completely dispensing with the unrealistic electron-gas approximation used by UM and Ueda to arrive at the final expression for the dynamical susceptibility.

Out of the weak itinerant-electron ferromagnets known in the literature [9], the intermetallic compound Ni_3Al has attracted the maximum attention. The ordered Ni_3Al phase has a homogeneity range that extends from 73 at.% Ni to 77 at.% Ni and, as the Ni concentration (x) increases from 73 at.%, long-range ferromagnetic order sets in at the critical concentration (boundary) $x_c \approx 74.5$ at.%. Early investigations of electrical resistivity [10], $\rho(T)$, and magnetoresistance (MR) [11, 12] in the polycrystalline samples of Ni_xAl_{100-x} alloys with x ranging from 73.5 to 76.0 at.% revealed the following. (I) In the temperature interval 1.2 K $\leqslant T \leqslant$ 4.2 K, $\rho(T)$, for all the compositions in the range specified above, is described by the expression [10] $\rho(T, x) = \rho(0, x) + A(x)T^{\alpha(x)}$. The exponent, $\alpha(x)$ (coefficient, $A(x)$) starts with a value $\alpha = 2.0$ ($A \cong 1.5$ nΩ cm K^{-2}) at $x =$ 73.5 at.%, goes through a minimum, $\alpha = 1.5$ (peak, $A \cong 12.0$ nΩ cm K$^{-\alpha(x_c)}$) at x_c and assumes the value of $\alpha = 2.0$ ($A \cong 7.0$ nΩ cm K$^{-\alpha(x)}$) at $x = 75.7$ and 76.0 at.%; at the stoichiometric composition $x = 75.0$ at.%, $\alpha = 1.75$ while A exhibits a discontinuous jump. Note that the observed variation of the exponent α with Ni concentration does not conform to that predicted by the above-mentioned theories [2–4]. (II) However, so far as the MR is concerned, the agreement between the experimental observations and the theoretical predictions, based on a two-(s–d) band model [11], is remarkably good [11, 12] over wide ranges of temperature and field in the strongly exchange-enhanced paramagnetic samples with $x < x_c$; a similar agreement between theory and experiment is observed [11, 12] in the weakly ferromagnetic compositions ($x > x_c$) only at low temperatures $T <$ 30 K and high fields $H >$ 100 kOe, where the negative MR (arising from the field-induced change in the density of states at the Fermi level of the d sub-bands) is masked by the 'conventional' positive MR due to the orbital motion of the conduction (s) electrons in a magnetic field (the so-called Lorentz force contribution). Subsequent studies [13–15] of electrical resistivity and magnetoresistance in this alloy system yielded results that are not only in conflict with one another but also with the previous ones [10–12]. For instance, Sasakura *et al* [13] observe a crossover from the T^2 variation of $\rho(T)$ in the range 1.2 K $\leqslant T \leqslant$ 2.5 K to the $T^{5/3}$ variation for temperatures 10 K $\leqslant T \leqslant T_C$, in polycrystalline ordered Ni_3Al. Yoshizawa *et al* [14] find that, irrespective of the Ni concentration (within the range 72.91 at.% $\leqslant x \leqslant$ 77.17 at.%), $\rho(T) \sim T^2$ at temperatures in the range 4.2 K $\leqslant T \leqslant$ 10 K in polycrystalline Ni_xAl_{100-x} alloys while Fuller *et al* [15] report that $\rho(T) \sim T^{5/3}$ from 1.2 K to $T = T_C$ in $Ni_{76.6}Al_{23.4}$ single crystal. Though these observations are at variance with one another, it is claimed that the temperature variations of magnetization, ρ and MR [13, 14] (ρ and magnetization [15]) are consistent with the predictions of the SCR spin fluctuation theory [4, 5].

Considering that a varying degree of site disorder, resulting from different annealing treatments, is bound to be present in the samples studied previously in the literature, it is possible that the above discrepancy between the experimental observations and hence between experiment and theory is caused by an interplay between site disorder and compositional disorder. We have, thus, undertaken a systematic experimental study, which aims at ascertaining the influence of off-stoichiometry (compositional disorder) and site disorder on the variations of resistivity and magnetoresistance with temperature in $Ni_{75}Al_{25}$. To this end, polycrystalline samples of Ni_xAl_{100-x} alloys with x ranging from 74 to 76 at.% were prepared out of a specific batch of high-purity Ni and Al under identical conditions without subjecting them to any thermal treatment. The observed compositional dependence of the transport and magneto-transport properties is thus governed by the compositional disorder (off-stoichiometry) and the site disorder introduced by the preparation protocol. The terms 'compositional disorder' and 'site disorder' are defined in section 2.2. A comparison between the results obtained on as-quenched samples (which have both site disorder and compositional disorder) and annealed/completely ordered counterparts (which have only compositional disorder) of a given composition is expected to bring out the effect of only the site disorder.

Table 1. Actual composition, Curie temperature, resistivity values at 1.7 and 300 K, and residual resistivity ratio (RRR).

Sample label	Actual Ni concentration (at.%)	T_C (K) $\rho(T)$	T_C (K) $\Delta\rho_\parallel(T)/\rho(T)$	ρ(1.7 K) ($\mu\Omega$ cm)	ρ(300 K) ($\mu\Omega$ cm)	RRR = $\rho(300\,K)/\rho(1.7\,K)$
ap-$Ni_{74.3}$	74.06(5)	41(1)	41(1)	7.62	41.30	5.42
	74.26(9)	48.5(9)	48(2)			
ap-$Ni_{74.8}$	74.82(8)	59(1)	60(1)	9.11	44.89	4.93
ap-$Ni_{75.1}$	75.08(8)	55.5(8)	55(1)	6.83	45.24	6.62
an-$Ni_{75.1}$	75.08(8)	56.1(9)	56(1)	7.08	51.97	7.34
ap-$Ni_{76.1}$	76.13(5)	71(1)	70(1)	14.80	70.68	4.77

2. Synthesis and characterization

2.1. Sample preparation and compositional analysis

Polycrystalline rods of 100 mm length and 10 mm diameter with nominal composition $Ni_{74}Al_{26}$, $Ni_{74.5}Al_{25.5}$, $Ni_{75}Al_{25}$ and $Ni_{76}Al_{24}$ were prepared by first melting the proper proportions of the 99.998% pure Ni and Al starting materials using a radio-frequency induction-melting technique and then quenching the melt following a procedure detailed elsewhere [16]. Samples in the shape of a disc of 10 mm diameter and 5 mm thickness, a rectangular strip of dimensions 9 × 2 × 0.5 mm^3 and a sphere of 2.5 mm diameter were spark-cut from these rods for x-ray diffraction, electrical and galvanomagnetic transport and magnetic measurements, respectively. The actual chemical composition of the samples, as determined by the x-ray fluorescence technique and inductively coupled plasma optical emission spectroscopy, is given in table 1. The compositional analysis also revealed that the total concentration of magnetic 3d transition metal impurities such as Mn, Cr, Fe and Co lies below 0.002 at.%. The 'as-prepared' alloy samples are henceforth labelled as ap-$Ni_{74.3}$, ap-$Ni_{74.8}$, ap-$Ni_{75.1}$ and ap-$Ni_{76.1}$. Optical polarizing micrographs and scanning electron micrographs of ap-$Ni_{74.3}$, ap-$Ni_{74.8}$ and ap-$Ni_{75.1}$ revealed the existence of a *trace* second crystalline phase. EDAX (energy-dispersive absorption of x-rays) analysis showed that (i) in the alloy ap-$Ni_{74.3}$, the second (minor) phase is *poorer* in Ni concentration (by ≅0.2 at.%) compared to the matrix (major) phase (which has the same composition as that given in table 1) and (ii) this difference in the composition of the minor and major crystalline phases diminishes very fast as the Ni concentration increases beyond 74.3 at.%, so much so that it falls within the uncertainty limits of the EDAX technique (≅±0.05 at.%) for the alloys with $x \geqslant 74.8$ at.%.

2.2. X-ray diffraction

X-ray diffraction patterns of the disc-shaped samples were recorded at room temperature over the scattering angle, 2θ, range of $10° \leqslant 2\theta \leqslant 120°$, using Co K$\alpha$ radiation, on an Inel x-ray diffractometer with curved position-sensitive detector. Since the scattered x-ray intensity is measured simultaneously over the entire 2θ range, even the weakest Bragg peaks, which would have normally escaped detection in the conventional x-ray diffractometers, can be detected with ease. Figure 1 compares the x-ray diffraction (XRD) patterns observed for the

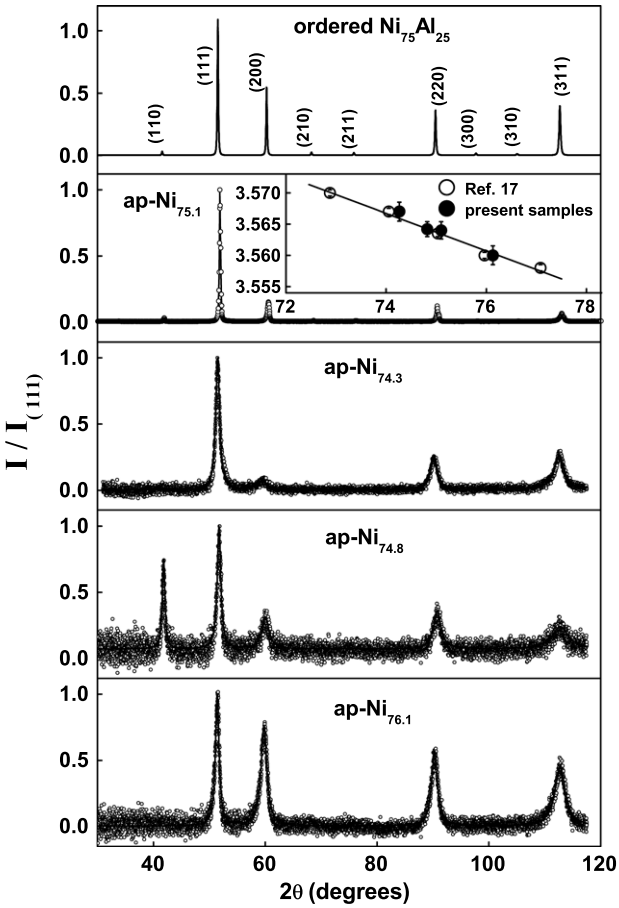

Figure 1. X-ray diffraction patterns taken at room temperature on the 'as-prepared' Ni_xAl_{100-x} alloys with $x = 74.3$, 74.8, 75.1 and 76.1 at.%. The top panel shows the x-ray pattern for a completely ordered Ni_3Al compound generated by the Rietveld programme. In order to facilitate a direct comparison between different compositions, the scattered x-ray intensities are normalized to the peak intensity of the (111) Bragg reflection. The inset shows the variation of the lattice parameter a with Ni concentration. Similar data on well-ordered Ni_xAl_{100-x} alloys reported previously in [17] are also included for comparison.

samples ap-$Ni_{74.3}$, ap-$Ni_{74.8}$, ap-$Ni_{75.1}$ and ap-$Ni_{76.1}$ with those generated for a completely ordered Ni_3Al compound using the space group $L1_2$ and the reported value [17, 18] of the lattice parameter a in the Rietveld programme. In a completely ordered Ni_3Al compound, Ni and Al atoms respectively occupy the face-centred and corner sites of the cubic unit cell. The

face-centred (corner) sites thus constitute the Ni (Al) sub-lattice. A complete atomic order in $Ni_{75}Al_{25}$ alloy exists only when 100% of Ni (Al) sub-lattice sites are occupied by Ni (Al) atoms. By the same token, *the maximum atomic order permitted by the chemical composition* in $Ni_{74}Al_{26}$ ($Ni_{76}Al_{24}$) alloy is realized only when 98.7%, 1.3% (100% and 0%) of Ni sub-lattice sites and 0%, 100% (4% and 96%) of Al sub-lattice sites are occupied by Ni and Al atoms. Antisite atoms, e.g. Ni (Al) atoms on Al (Ni) sub-lattice sites, on either of, or both, the sub-lattices give rise to site disorder in the atomic arrangement of the underlying face-centred-cubic (fcc) lattice. Thus, a *residual site disorder* (e.g. 1.3% (4%) of Ni (Al) sites occupied by Al (Ni) atoms in $Ni_{74}Al_{26}$ ($Ni_{76}Al_{24}$) alloy) is *intrinsic* to off-stoichiometric alloys that exhibit maximum possible atomic order. This type of residual site disorder that depends on chemical composition will henceforth be referred to as the *compositional disorder*. Additional site disorder brought about by the variation in the population of antisite atoms on Ni and Al sub-lattices in an alloy of given composition will be simply termed as the *site disorder*. The existence of well-defined Ni and Al sub-lattices in an ordered Ni_xAl_{100-x} alloy gives rise to the superstructure Bragg peaks corresponding to the reflections (110), (210), (211), (300), (310), etc, besides the fundamental Bragg reflections (111), (200), (220), (222), (311), etc, that are characteristic of the fcc structure. The ratio of the integrated intensities of the superstructure and fundamental Bragg peaks is a direct measure [16] of the atomic order (or disorder) present in a given alloy. The comparison between the observed and generated XRD spectra in figure 1 brings out the following features. Except for the appearance of the (110) reflection in the $Ni_{74.8}$ sample presumably due to the texture effects, the superstructure Bragg peaks are completely absent. A complete absence of superstructure Bragg peaks reflects a large population of antisite atoms on Ni and Al sub-lattices and hence the presence of a substantial amount of site disorder in all the samples. The XRD linewidths are considerably broader compared to those in the ordered stoichiometric compound. The extra broadening possibly originates from a large local internal strain at the grain boundaries and/or local compositional inhomogeneity (e.g. a minor second isostructural phase with a slightly different lattice parameter)/site disorder. For a given Bragg peak, the linewidth decreases as the Ni concentration increases. This observation is consistent with the expected progressive enhancement in the compositional disorder as the critical concentration [16] $x_c \approx 73.5$ at.% is approached from above. The analysis of the observed XRD patterns reveals that the lattice parameter a decreases linearly with increasing Ni concentration (inset of figure 1) in much the same way as that reported previously [17] on well-ordered Ni_xAl_{100-x} alloys. The finding that the functional form of $a(x)$ is the same for site-disordered and ordered Ni_xAl_{100-x} alloys asserts that site disorder has essentially no effect on the lattice parameter and that the observed variation of a with x is solely governed by the compositional disorder.

2.3. Electrical resistivity and magnetoresistance

Electrical resistivity, $\rho(T)$, and longitudinal magnetoresistance, $\Delta\rho_\parallel/\rho = [\rho_\parallel(T, H) - \rho(T, H = 0)]/\rho(T, H = 0)$, were measured to a relative accuracy of better than 10 ppm on rectangular strips of 10 mm length, 2 mm width and 0.5 mm thickness, at temperatures in the range 1.7 K $\leqslant T \leqslant$ 300 K, using a four-probe dc method; $\Delta\rho_\parallel/\rho$ measurements were carried out in the above temperature range in external magnetic fields, H, up to 80 kOe. In this paper, the magnetoresistance versus magnetic field isotherms taken on the Ni_xAl_{100-x} alloys in different temperature regimes have been analysed in terms of the relevant theoretical expressions yielded by the self-consistent spin fluctuation theory [8] using the magnetization, $M(T, H)$, data taken on the samples coming from the same batch as that used in this work. The results of an elaborate analysis of the $M(T, H)$ data and their discussion in terms of the spin fluctuation theory [19] form the subject of the following paper (henceforth referred to as paper II).

3. Results and discussion

With a view to resolving the controversial issues concerning the electrical and galvanomagnetic transport in weakly ferromagnetic metals detailed in the introductory section, a quantitative comparison between theory [8] and experiment is made in this section. To facilitate such a comparison, we quote the relevant results of the *self-consistent* calculation [8] of spin-wave and exchange-enhanced spin-density fluctuation contributions to the electrical resistivity, $\rho(T)$, and magnetoresistance (MR) of weak itinerant-electron ferromagnets, and refer the reader to [8] for details.

At $T = 0$, the energy dispersion, $E(q)$, of magnetic excitations in a weakly ferromagnetic metal consists of a small region around $q = 0$ in the Brillouin zone, where the bound states for electron–hole pairs, representing spin-wave excitations, have lower energy and are separated by an energy gap from the energy continuum, corresponding to the Stoner single-particle spin-flip excitations. This energy gap reduces as q increases such that beyond a certain threshold value of $q = q_0$, the spin-wave dispersion curve enters the Stoner excitation continuum with the result that *propagating transverse* spin fluctuations (spin waves) get damped. For $q > q_0$, the magnetic excitations in the continuum are the overdamped (*non-propagating*) modes of exchange-enhanced longitudinal and transverse spin-density fluctuations. Since spin-wave modes of larger and larger q are excited as the temperature is raised from $T = 0$, the transition at $q = q_0$ from well-defined spin waves to *non-propagating* exchange-enhanced *transverse* spin fluctuations manifests itself at a certain finite value of temperature in the measurement of $\rho(T)$ and MR. In contrast, the thermally excited *non-propagating* exchange-enhanced *longitudinal* spin-density fluctuations persist down to $q = 0$ and coexist with, but are swamped by, spin waves for $q \leqslant q_0$.

At low temperatures ($T \ll T_C$), the main contribution to $\rho(T)$ and MR arises from long-wavelength ($q \leqslant q_0$) low-frequency spin-wave (SW) modes. These SW

contributions to the 'zero-field' resistivity, $\rho_{SW}(T, H = 0)$, and magnetoresistance, $(\Delta\rho/\rho)_{SW}$, are given by [8]

$$\rho_{SW}(T, H = 0) = \frac{\pi}{3}\rho_0\Gamma(2)\zeta(2)\left(\frac{g\mu_B M}{\hbar}\right)\left(\frac{k_B T}{D}\right)^2 \quad (1)$$

and

$$\left(\frac{\Delta\rho}{\rho}\right)_{SW} = \frac{\rho_{SW}(T, H)}{\rho_{SW}(T, H = 0)} - 1 = [\Gamma(3)\zeta(2)]^{-1} \times \left[h\ln(e^h - 1) + 2\sum_{n=1}^{\infty}\frac{(-1)^n(e^h - 1)^n}{n^2}\right] \quad (2)$$

for $(e^h - 1) < 1$, where the *reduced field*, $h = (g\mu_B H/k_B T)$. In order to make the variations of $(\Delta\rho/\rho)_{SW}$ with h more transparent, the $(e^h - 1)$ term, appearing in equation (2), is *approximated* by h for $h \ll 1$ and only the first two (leading) terms in the sum over n are retained, with the result that

$$\left(\frac{\Delta\rho}{\rho}\right)_{SW} \cong 0.304\left[h\ln h - 2h + \frac{1}{2}h^2\right]. \quad (3)$$

At intermediate temperatures, $T \ll T_C$, the spin fluctuation (SF) contribution to $\rho(T, H = 0)$ or MR becomes more important than the SW contribution. At such temperatures, the longitudinal and transverse SF contributions to $\rho(T, H = 0)$, and hence to MR, have to be treated differently since the imaginary part of the dynamical wavevector-dependent spin susceptibility has different lower bounds $(q_\perp = q_0, \omega = 0)$ and $(q_\parallel = 0, \omega = 0)$ in the (q, ω) plane for the transverse and longitudinal spin fluctuations. Using the expressions for the temperature- and field-dependent *longitudinal* $(\chi_\parallel = \partial M/\partial H)$ and *transverse* $(\chi_\perp = M/H)$ susceptibilities that are *consistent* with the *magnetic equation of state* $H = AM(T, H) + b[M(T, H)]^3$, this theoretical approach leads to the final result [8]

$$\rho_{SF}(T, H = 0) = \rho_\parallel(T, H = 0) + \rho_\perp(T, H = 0) = \frac{\pi^2}{9}\rho_0\gamma\left(\frac{k_B T}{\hbar\Gamma}\right)^2\left[\frac{\pi}{2\sqrt{2}}\sqrt{\frac{c}{b}}\frac{1}{M_0} + \frac{4}{q_0}\right] \quad (4)$$

and

$$\left(\frac{\Delta\rho}{\rho}\right)_{SF} = \frac{\rho_{SF}(T, H)}{\rho_{SF}(T, H = 0)} - 1 = \left[\frac{\pi}{2\sqrt{2}}\sqrt{\frac{c}{b}}M_0^{-1} + \frac{4}{q_0}\right]^{-1} \times \left[\frac{\pi}{2}\sqrt{\frac{c}{b}}\left(3M^2 - M_0^2\right)^{-1/2} + \frac{4}{q_0}\left(1 - \frac{2}{3a} \times \left[b(M^2 - M_0^2)\right] + \frac{3}{5a^2}[b^2(M^2 - M_0^2)^2]\right)\right] - 1 \quad (5)$$

where $M_0 \equiv M(T, H = 0) = (-A(T)/b)^{1/2}$ and $M \equiv M(T, H)$ are spontaneous and 'in-field' magnetizations, $a = 1/q_0^2 c$ and the detailed expressions for the coefficients $A(0)$, b and c are given in [8] and [19].

At temperatures just outside the critical region but on either side of the Curie point, T_C (henceforth referred to as 'for temperatures close to T_C', for brevity), the following analytical expressions for the SF contributions to the $\rho(T, H = 0)$ and MR are obtained [8] by using the *classical approximation* [8] and taking into account the functional dependences of the SF cutoff wavevector q_c on temperature and field:

$$\rho_{SF}(T, H = 0) = \frac{\pi}{2}\eta\rho_0\gamma\left(\frac{k_B T}{\hbar\Gamma}\right)^{5/3}\left[1 - 2\psi M_0^2 + 4\phi M_0^4\right] \quad (6)$$

and

$$\left(\frac{\Delta\rho}{\rho}\right)_{SF} = \frac{\rho_{SF}(T, H)}{\rho_{SF}(T, H = 0)} - 1 = \left\{1 - \psi[(3M^2 - M_0^2) + 2(M^2 - M_0^2)] + \phi[(3M^2 - M_0^2)^2 + 2(M^2 - M_0^2)^2]\right\} \left\{1 - 2\psi M_0^2 + 4\phi M_0^4\right\}^{-1} - 1 \quad (7)$$

where $\psi = \alpha b$ and $\phi = \beta b^2$. For the detailed definitions of the band parameters b, c, γ and Γ, and those of other quantities appearing in equations (1)–(7), such as α, β, η and ρ_0, the reader should refer to [8].

The above-mentioned parameters are specific to a given weakly ferromagnetic metal and hence they will sensitively depend on the Ni concentration, x, in the present case. Another important point to note is that, with increasing compositional disorder or increasing external pressure (i.e. as $x \to x_c$ or $p \to p_c$), $T_C \to 0$ and the energy gap at $q = 0$ between the Stoner energy continuum and the bound states, representing spin-wave excitations, narrows down tremendously so much so that the spin-wave dispersion region near $q = 0$ in the Brillouin zone progressively shrinks to an extremely small size. Consequently, near $x = x_c$, the spin-wave dispersion curve enters the Stoner excitation continuum at $q_0 \approx 0$ and a transformation from the *propagating transverse* spin fluctuations (spin waves) to overdamped (*non-propagating*) modes of exchange-enhanced longitudinal and transverse spin-density fluctuations occurs as soon as q exceeds $q_0 \approx 0$. Thus, strong departures from the spin-wave behaviour are expected at low temperatures as x nears x_c. Though the theoretical calculations detailed in [8] do not explicitly take into account the effect of site disorder, site disorder is expected to enhance the above-stated effect of compositional disorder.

Electrical resistivity, $\rho(T)$, is plotted against temperature from 1.7 to 300 K in figure 2. The inset of figure 2 displays the temperature variation of the temperature derivative of resistivity, $d\rho(T)/dT$. $d\rho(T)/dT$ goes through a peak (two peaks) at a temperature, $T = T_{peak}$, for the alloys with $x = 76.1$, 75.1 and 74.8 at.% ($x = 74.3$ at.%). Identifying T_{peak} with the Curie temperature, T_C, yields the values of T_C for different compositions given in table 1. Consistent with the EDAX results, in the case of ap-$Ni_{74.3}$ sample alone, the presence of a minor second isostructural phase with Ni concentration $x = 74.06(4)$ (table 1) is reflected in a satellite peak at $T_C = 41$ K in $d\rho(T)/dT$ (top inset of figure 2(a)); the main peak at $T_C = 48$ K corresponds to the major crystalline phase with $x = 74.3$ at.%. Residual resistivity ratio, $\rho(300\text{ K})/\rho(1.7\text{ K})$, (RRR) and residual resistivity at 1.7 K, $\rho(0)$, as functions of Ni concentration are displayed in table 1 and figure 3. Of all the 'as-prepared' (ap) samples, the sample of stoichiometric composition ($x = 75.1$ at.%) has the lowest (highest) residual resistivity (RRR). Annealing the ap-$Ni_{75.1}$ sample at 520 °C for 16 days improves the atomic order from 75% to nearly [16] 85%, leaves the residual resistivity

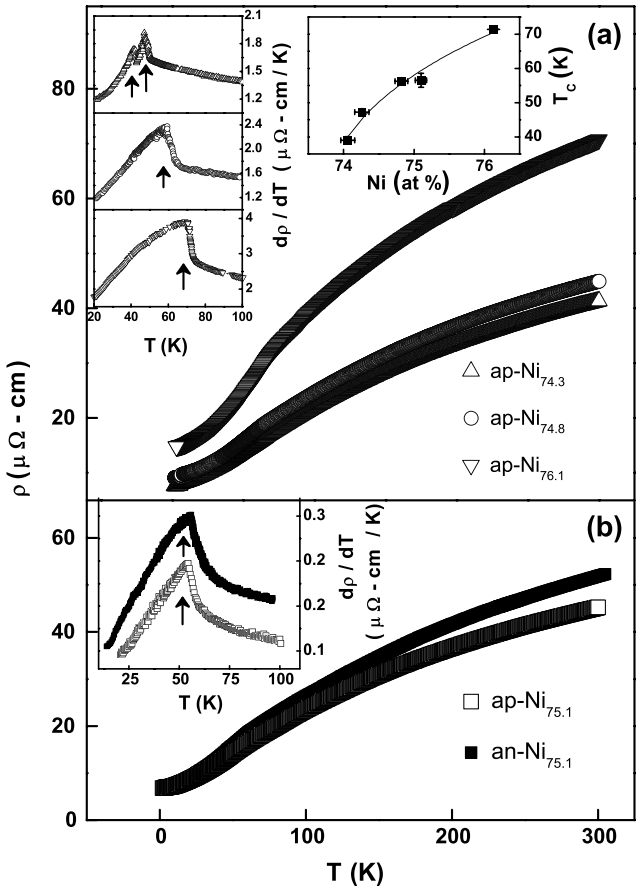

Figure 2. Electrical resistivity, ρ, as a function of temperature from 1.7 to 300 K. Insets show the temperature derivative of resistivity, $\mathrm{d}\rho/\mathrm{d}T$, plotted against temperature. The arrows indicate approximate locations of the peak temperature, which is identified with the Curie temperature, T_C. Top right insert highlights the Ni concentration dependence of T_C.

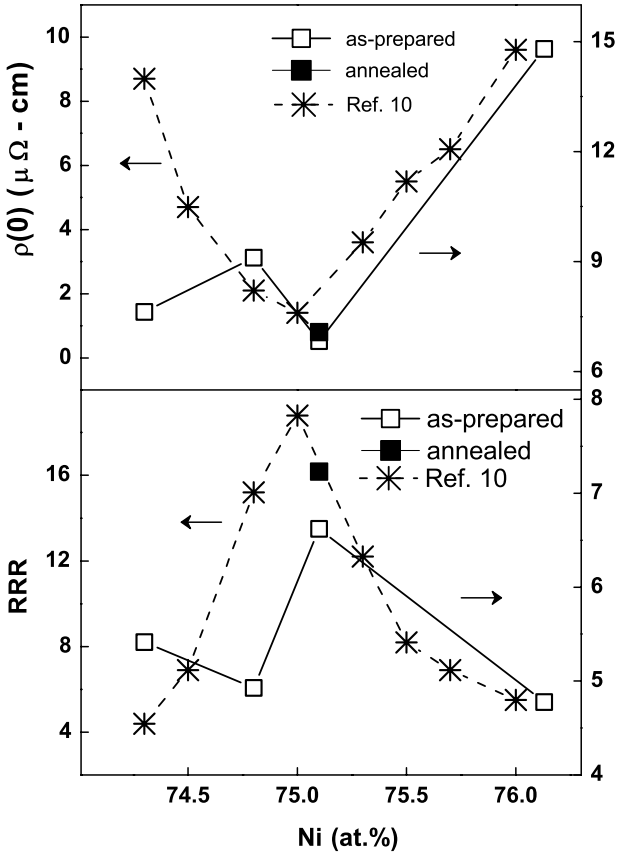

Figure 3. Variation of the residual resistivity, $\rho(0)$, and residual resistivity ratio (RRR) with Ni concentration. The corresponding data on well-ordered samples, previously reported in [10], are also included for comparison.

essentially unaltered but increases the RRR appreciably. A much lower annealing temperature, $T_\mathrm{A} = 520\,^\circ$C (as against $T_\mathrm{A} = 1150\,^\circ$C, used in the literature [10] to achieve ≈100% atomic order), was chosen to avoid a significant loss of Al in the alloy during annealing so that no shift in the composition occurs and a comparison between the physical properties of the 'as-prepared' and 'annealed' samples brings out clearly the role of site disorder. Comparison with the data reported by Fluitman *et al* [10] on *completely ordered* samples in the alloy series $\mathrm{Ni}_x\mathrm{Al}_{100-x}$ (note the widely different sensitivities of the ordinate scales for different sets of data in figure 3) indicates that the as-prepared samples in the present study have a considerable amount of site disorder. The variations of longitudinal magnetoresistance, $\Delta\rho_\parallel(T, H)/\rho(T, H = 0)$, with temperature at various fixed values of the external magnetic field, H, in the temperature interval 3 K $\leqslant T \leqslant$ 200 K, shown in figure 4, are representative of the '*as-prepared*' and '*annealed*' (an) $\mathrm{Ni}_{75.1}$ samples as well. Magnetoresistance (MR) is *negative* in the entire temperature range extending from 3 to 300 K and goes through a *maximum* as a function of temperature at $T = T_\mathrm{max}$. The values of T_max are also tabulated in table 1. For a given alloy composition, $T_\mathrm{max} \cong T_\mathrm{C}$.

3.1. Low temperatures ($T \ll T_C$)

Figure 5(a) clearly demonstrates that, at temperatures 1.7 K $\leqslant T \leqslant T_x$ (where T_x depends on the Ni concentration, x), $\rho(T)$ is accurately described by the expression $\rho(T) \equiv \rho(T, H = 0) = \rho(T = 0, H = 0) + A_n(H = 0)T^n$ with the values of the exponent n as 1.50(1), 1.66(1), 1.64(2) and 1.80(5) for the samples ap-$\mathrm{Ni}_{74.3}$, ap-$\mathrm{Ni}_{74.8}$, ap-$\mathrm{Ni}_{75.1}$ and an-$\mathrm{Ni}_{75.1}$, respectively. These samples exhibit a *strong departure* from the *Fermi liquid behaviour* at low temperatures in that the above values of the exponent n are significantly different from that ($n = 2$) predicted by the Fermi liquid theory. By contrast, $\rho(T)$ in the ap-$\mathrm{Ni}_{76.1}$ follows the T^2 law (the Fermi liquid behaviour) over a narrow temperature range 1.7 K $\leqslant T \leqslant$ 16 K. As the critical concentration [16] $x_\mathrm{c} \cong 73.5$ at.% (site disorder reduces the critical concentration from $x_\mathrm{c} \cong 74.6$ at.% to $x_\mathrm{c} \cong 73.6$ at.%, see below) is approached from above, the *deviations* from the Fermi liquid behaviour become *more prominent* and the temperature range (1.7 K $\leqslant T \leqslant T_x$ with $T_x = 25$ K ($T_x = 21$ K) for ap-$\mathrm{Ni}_{74.3}$ and ap-$\mathrm{Ni}_{74.8}$ (ap-$\mathrm{Ni}_{75.1}$)) over which the non-Fermi liquid behaviour persists *widens*. The values of the exponent n and coefficient $A_n(0) \equiv A_n(H = 0)$ are determined by the 'range-of-fit' analysis, in which the values of the parameters $\rho(0) \equiv \rho(T = 0, H = 0)$, $A_n(0)$ and n are monitored as the temperature range of the fit (based on the above expression) is varied.

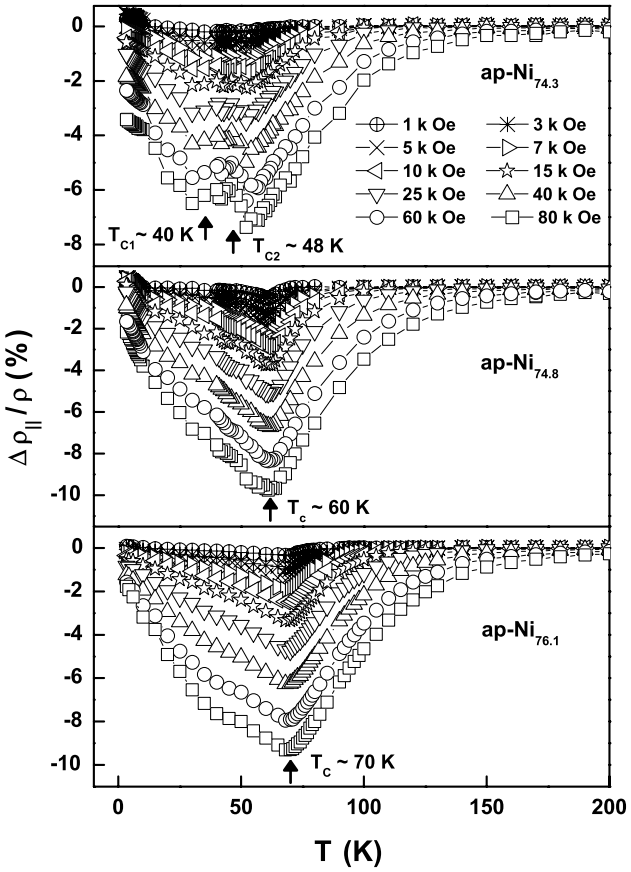

Figure 4. Longitudinal magnetoresistance, $\Delta\rho_{\parallel}/\rho$, as a function of temperature at fixed values of the external magnetic field. The arrows indicate the approximate location of the Curie temperature, T_C, where $\Delta\rho_{\parallel}(T, H)/\rho(T, H = 0)$ goes through a dip at low fields.

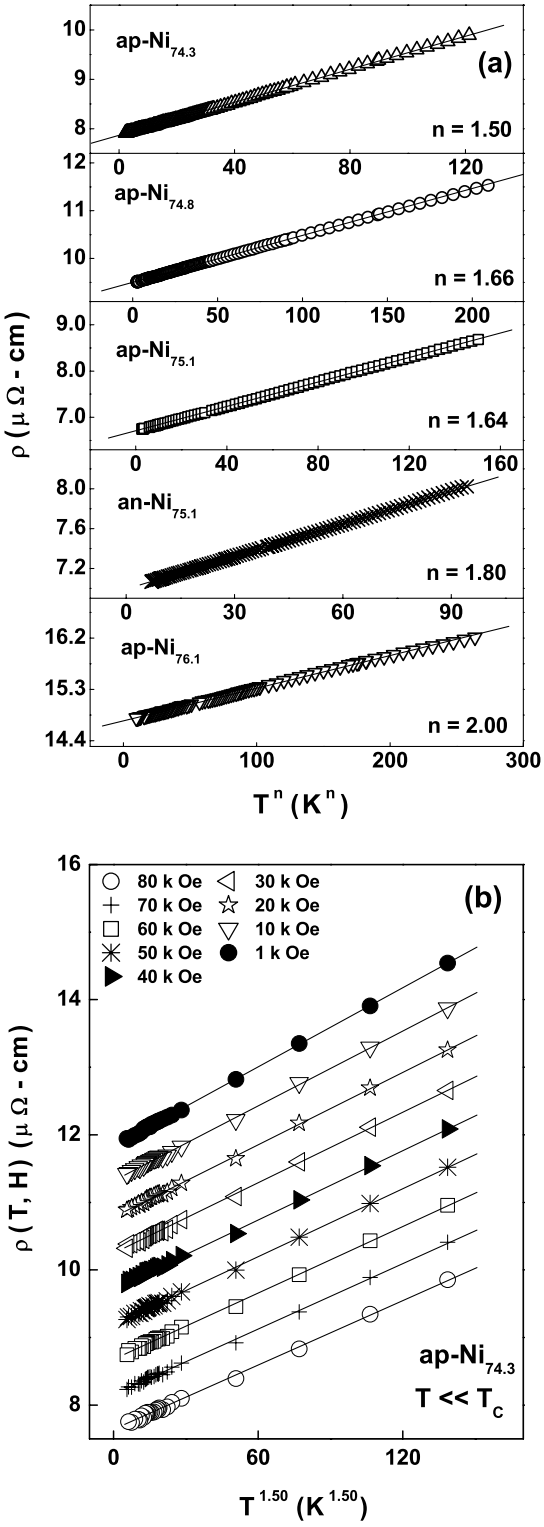

Figure 5. (a) Non-Fermi (Fermi) liquid behaviour of resistivity at low temperatures in ap-$Ni_{74.3}$, ap-$Ni_{74.8}$, ap-$Ni_{75.1}$ and an-$Ni_{75.1}$ (ap-$Ni_{76.1}$). (b) $T^{1.5}$ variation of $\rho(T, H)$ for the sample ap-$Ni_{74.3}$ at different fixed fields at low temperatures. For the sake of clarity, a constant upward shift of 0.5 $\mu\Omega$ cm has been given to the successive $\rho(T, H)$ data starting from that taken at $H = 80$ kOe.

The values of $\rho(0)$, $A_n(0)$ and n, so determined over the specified temperature ranges, are given in table 2. At this stage, it is interesting to note the following observations. (a) The $T^{1.65}$ variation of $\rho(T)$ at $T \leqslant 7$ K and ambient pressure has also been reported [20] in single crystals of Ni_3Al. (b) The value of the exponent n falls below [21] $n = 2$ and goes on decreasing continuously, when the upper bound T_m of the temperature interval 0.05 K $\leqslant T \leqslant T_m$, at a given external pressure in the range 32 kbar $\leqslant p \leqslant$ 99 kbar, is increased from 1 to 5 K or when, at a fixed value of T_m, the external pressure is increased from 32 to 99 kbar. The presently determined values of the ratio $A_n(0)/\rho(0)$ and the exponent n for different Ni concentrations, x, are compared in figure 6 with those reported earlier [10] for similar compositions. The quantities $A_n(0, x)/\rho(0, x)$ and $n(x)$ exhibit the same trend in the present case as that observed previously [10]; however, our values for $A_n(0, x)/\rho(0, x)$ are lower by nearly a factor of two, particularly for x close to the stoichiometric composition. Considering that the samples used in [10] had been subjected to prolonged annealing at elevated temperatures so as to ensure complete atomic ordering in them, the reduced $A_n(0, x)/\rho(0, x)$ (or RRR) in our 'as-prepared' samples can be attributed to a high degree of site disorder present in them. The exponent n increases from $n = 1.64(3)$ to 1.80(5) when the ap-$Ni_{75.1}$ sample is annealed. An excellent agreement between the value $n = 1.80(5)$ for the annealed (ordered) $Ni_{75.1}$ and that [10] ($n = 1.75$) for the completely ordered Ni_3Al compound leads to the obvious conclusion that site

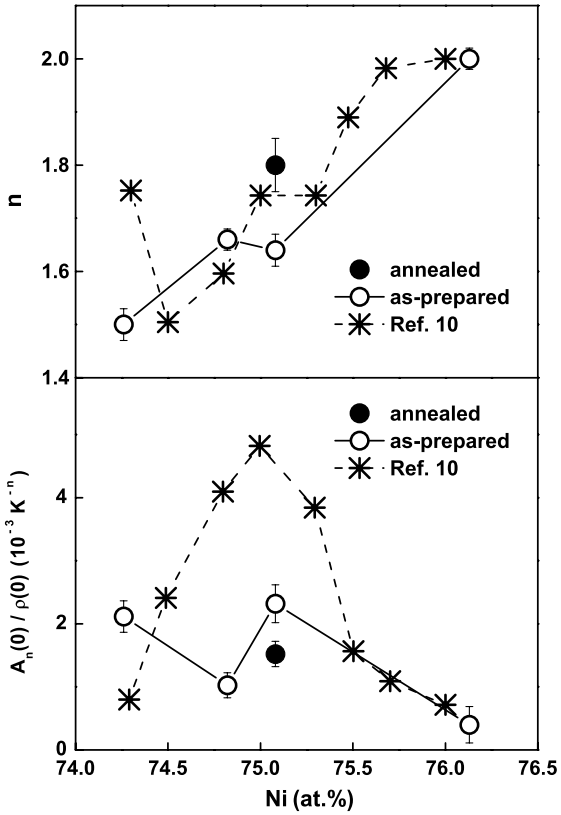

Figure 6. The variations of the exponent n and the ratio $A_n(0)/\rho(0)$ with Ni concentration at low temperatures. The corresponding data on well-ordered samples, previously reported in [10], are also included for comparison.

disorder tends to enhance the deviations from the Fermi liquid behaviour at the stoichiometric composition. Fluitman *et al* [10] report the critical nickel concentration x_c for the onset of long-range ferromagnetic order as $x_c = 74.6$ at.%, which is well above $x_c = 73.6$ at.% obtained in the present case when the $T_C(x)$ data are fitted to the simple power law $T_C(x) = t_p(x - x_c)^p$ with $p = 0.33$ (top inset in figure 2(a)). The site disorder thus lowers the critical Ni concentration (for details, see paper II).

From a close comparison of the non-Fermi liquid behaviour in the single crystals, completely ordered and site-disordered polycrystalline samples with Ni concentration close to the critical concentration x_c, we infer that the effect of site disorder is (i) to make the non-Fermi liquid behaviour more prominent, particularly in the stoichiometric composition by increasing the extent of deviation of the exponent n from the value $n = 2$ and (ii) to stabilize the non-Fermi liquid behaviour in any given composition over a much wider temperature range.

Before discussing the present results in the light of the existing theories, the following remarks about a comparison between theory and experiment are in order. For $x \cong x_c$ (or, equivalently, externally applied pressures, p, in the immediate vicinity of the critical pressure [21], p_c), $T_C \approx 0$ so that at ultra-low temperatures the conditions remain the same as those for temperatures close to T_C. Thus, by predicting the variation $\rho(0) \sim T^{5/3}$ at temperatures $T \approx T_C$, the theoretical treatment [8], like the SCR theory [4], adequately describes the non-Fermi liquid behaviour observed at ambient pressure for concentrations $x \cong x_c$ (figures 5(a) and 9) or for the stoichiometric composition at pressures $p \cong p_c$ [21]. For $x > x_c$ or $p < p_c$, T_C has an appreciable magnitude and these theories [4, 8] predict a T^2 variation of resistivity at low (intermediate) temperatures arising from the scattering of conduction electrons from *propagating transverse* spin fluctuations, i.e. spin waves, SW (exchange-enhanced longitudinal and transverse spin fluctuations). The electron–electron (EE) scattering too gives rise to the T^2 variation of resistivity at low temperatures (the Fermi liquid behaviour) but, unlike the SW scattering, the EE scattering is *insensitive* to H. A T^2 dependence of $\rho(T)$ has been earlier observed in a Ni_3Al single crystal [21] at low temperatures, $0.05\ K \leqslant T \leqslant 1\ K$, and low pressures, $p \ll p_c$, and presently in ap-$Ni_{76.1}$ (figure 5(a)) at ambient pressure and temperatures, $1.7\ K \leqslant T \leqslant 16\ K$. However, the theoretically predicted [4, 8] T^2 variation of $\rho(T)$ at low temperatures (basically originating from the spin-wave dispersion which is *quadratic* in the wavevector q) is *at variance* with the observed values 1.5–1.66 of the exponent n in the Ni concentration range $x_c < x \leqslant 75.1$ at.% (figures 5(a) and 6). In view of the above remarks, the non-Fermi liquid behaviour observed at low temperatures when x falls below 76.1 at.% (figure 6) most likely reflects that the increased compositional disorder (or increased external pressure) as the critical concentration, x_c (critical pressure, p_c), is approached from above (below) alters the spin-wave dispersion at *finite* q such that, as q increases from $q = 0$, the SW dispersion becomes increasingly similar to the spin fluctuation dispersion prevalent at temperatures close to T_C. Note that the effect of compositional disorder or increasing external pressure on the SW dispersion has been brought out clearly in the paragraph following equation (7).

The above proposition provides the following explanation for the monotonic reduction in the exponent n from $n = 2$ to 1.66 observed [21] in Ni_3Al when the upper bound, T_m, of the temperature range $0.05\ K \leqslant T \leqslant T_m$ increases from 1 to 5 K. At sub-Kelvin temperatures, only long-wavelength ($q \approx 0$) spin-wave modes get excited. In the long-wavelength ($q \to 0$) limit, the SW dispersion is quadratic in q and hence it is not surprising that $n = 2$ in the temperature range $0.05\ K \leqslant T \leqslant 1\ K$. As the temperature increases above 1 K, SW modes of larger and larger q (compared to $q = 0$) get thermally excited, with the result that the modified SW dispersion at such q values causes n to decline from the value $n = 2$. The magnetic field introduces a gap ($E_g = g\mu_B H_{eff}$; $H_{eff} = H - H_{dem} + H_A$) in the spin-wave energy spectrum. Creation of a gap makes it energetically more difficult to excite spin waves (or equivalently, at a given temperature, the spin-wave stiffness, D, increases steeply at low fields and tends to saturate at high fields in accordance with the relation [8, 19] $D(T, H) = g\mu_B M(T, H)c_\perp$). Consequently, an increase in H progressively suppresses the SW scattering contribution, thereby reducing the resistivity and giving rise to *negative magnetoresistance*, in agreement with our observations (figure 4). However, H does not alter the q

Table 2. Temperature ranges and the parameter values corresponding to the fits in the low temperature (spin-wave) region, based on the relation $\rho(T) = \rho(0) + A_n(0)T^n$ and equation (8) of the text.

Sample label	Temperature range (K)	$\rho(0)$ ($\mu\Omega$ cm)	n	$A_n(0)$ (nΩ cm K^{-n})	$A_n^*(0)$ (nΩ cm K^{-n})	a_λ (10^{-4} Oe$^{-\lambda}$)	λ
ap-Ni$_{74.3}$	1.7–24 (0.04 T_C–0.50 T_C)	7.85(2)	1.50(1)	16.6(6)	16.5(2)	3.9(5)	0.52(2)
ap-Ni$_{74.8}$	1.7–25 (0.03 T_C–0.42 T_C)	9.50(1)	1.66(1)	9.74(6)	9.6(1)	2.8(3)	0.60(3)
ap-Ni$_{75.1}$	1.7–21 (0.03 T_C–0.38 T_C)	6.68(3)	1.64(3)	15.5(5)	14.8(9)	2.4(4)	0.65(5)
an-Ni$_{75.1}$	1.7–12.5 (0.03 T_C–0.22 T_C)	7.00(1)	1.80(5)	9.0(6)	8.3(3)	2.4(6)	0.65(3)
ap-Ni$_{76.1}$	1.7–16.25 (0.02 T_C–0.23 T_C)	14.73(3)	2.00(2)	5.88(5)	5.80(9)	2.6(6)	0.80(1)

dependence in the SW dispersion relation and hence the field has no effect on the temperature dependence of resistivity. This theoretical prediction [8] is clearly corroborated by the data, presented in figure 5(b), which are representative of all the compositions studied in this work. The coefficient $A_n(H)$ of the T^n term in the expression $\rho(T, H) = \rho(0, H) + A_n(H)T^n$ is calculated from the slope of the $\rho(T, H)$ versus T^n straight lines displayed in figure 5(b). That the functional dependence of A_n on H is accurately described by the empirical relation

$$A_n(H) = A_n^*(0)[1 - a_\lambda H^\lambda], \tag{8}$$

is clearly borne out by the $A_n(H)/A_n^*(0)$ versus H^λ plots shown in figure 7. While $A_n(H)$ is a quantitative measure of the suppression of SW scattering at a given field strength over a specified temperature range (table 2) at low temperatures, the term $a_\lambda H^\lambda$ gives how such a suppression varies with H. The optimum values of $A_n^*(0)$, a_λ and the exponent λ obtained from these plots for various compositions are given in table 2. The values of $A_n^*(0)$, so obtained, are the same as those ($A_n(0)$) directly determined from the 'zero-field' resistivity, $\rho(T)$, data (cf $A_n^*(0)$ and $A_n(0)$ listed in table 2). The $A_n(H)$ and $A_n(0)$ data with $n = 2$, reported by Yoshizawa *et al* [14] on well-ordered samples of similar composition (an-Ni$_{75.1}$ and an-Ni$_{76.1}$) are plotted in figure 7 as $A_n(H)/A_n(0)$ versus H^λ, using the presently determined values of the exponent λ (which are found to be consistent with their data), so as to facilitate a direct comparison with our data. While comparing the two sets of data, proper allowance has to be made for the change in $A_n(H)$ and $A_n(0)$ with n (the exponent of the T^n term in the expressions for $\rho(T, H)$ and $\rho(T, H = 0)$). Such a comparison reveals that, at any specified field value, site disorder reduces the extent of suppression by the field and this reduction in suppression (by site disorder) becomes more pronounced as H increases. Alternatively, for a *fixed* value of λ, *site disorder*, in a sample of given composition, *reduces* a_λ. The coefficient a_λ (exponent λ) decreases (increases) *linearly* with Ni concentration, as shown from the top panel of figure 7.

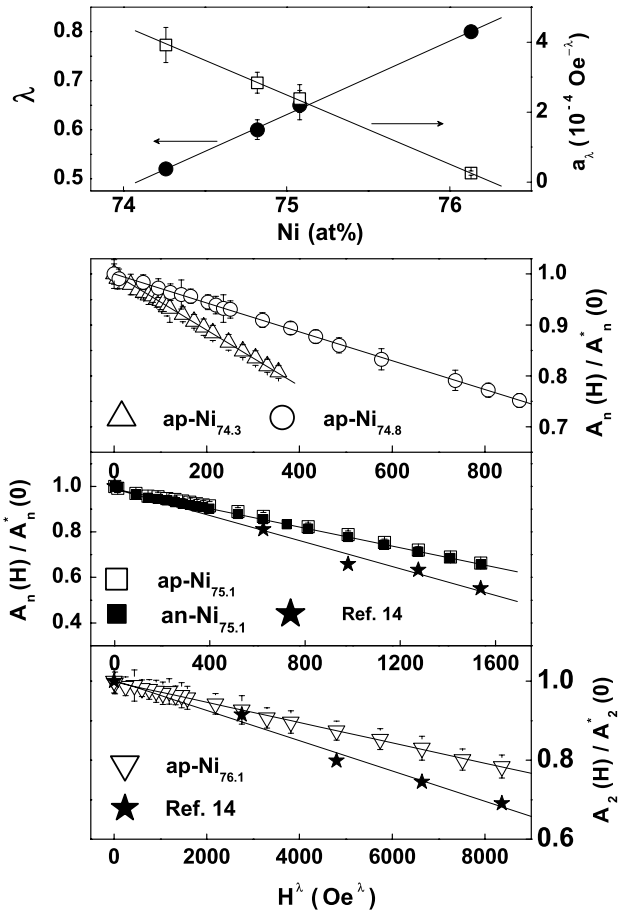

Figure 7. H^λ power law field dependence of the normalized coefficient, $A_n(H)/A_n^*(0)$, of the T^n term in the expression of resistivity at low temperatures. The corresponding data on well-ordered samples from [14] are also included for comparison. Top panel displays linear composition dependence of the exponent λ and coefficient a_λ of the magnetic field-dependent term in equation (8) of the text.

Contrasted with the above empirical relation, i.e. equation (6), which quantifies the suppression of SW scattering at a *given field strength over a specified temperature range* at low temperatures, the self-consistent treatment [8] calculates the suppression of SW scattering with *varying magnetic field at a fixed temperature* in the low temperature region. Thus, in order to verify the theoretical predictions [8], the fits to the $\Delta\rho_\parallel/\rho$ versus H isotherms taken in the spin-wave temperature region (the actual temperature range depends on the composition, see table 2) are attempted based on equation (3) by varying the coefficients of the $h \ln h$, h and h^2 terms so as to optimize agreement between the theory

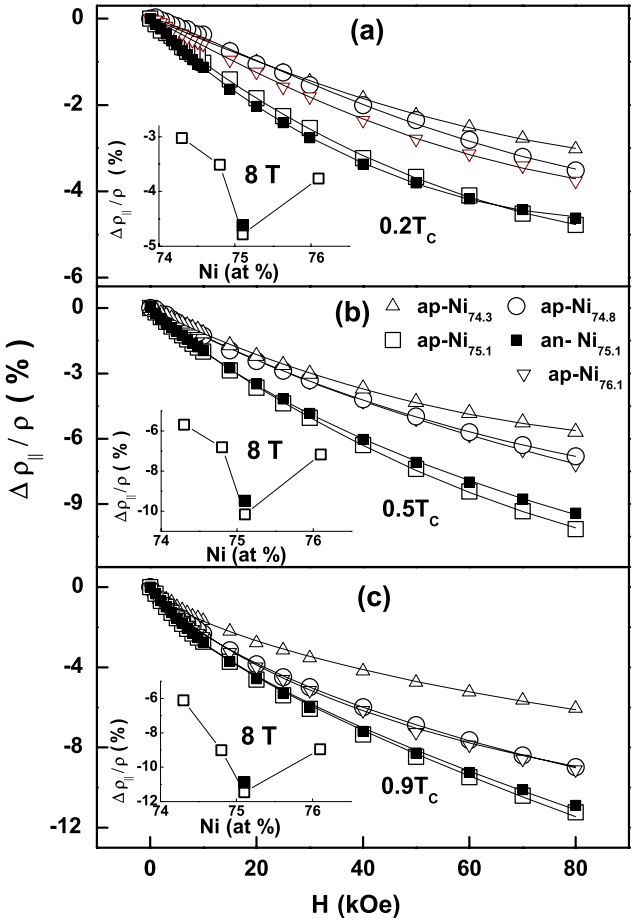

Figure 8. Longitudinal magnetoresistance, $\Delta\rho_\parallel/\rho$, of all the compositions as a function of magnetic field at $T = 0.2T_C$, $0.5T_C$ and $0.9T_C$. Open symbols denote the $\Delta\rho_\parallel/\rho$ data while the continuous curves through the data points at $T = 0.2T_C$, $0.5T_C$ and $0.9T_C$ are the theoretical fits based on equations (3), (5) and (7) of the text, respectively. Insets show that the longitudinal magnetoresistance, $\Delta\rho_\parallel/\rho$, at $H = 80$ kOe (or, in SI units, $H = 8$ T) and $T = 0.2T_C$, $0.5T_C$ and $0.9T_C$ goes through a dip at the stoichiometric composition as a function of Ni concentration.

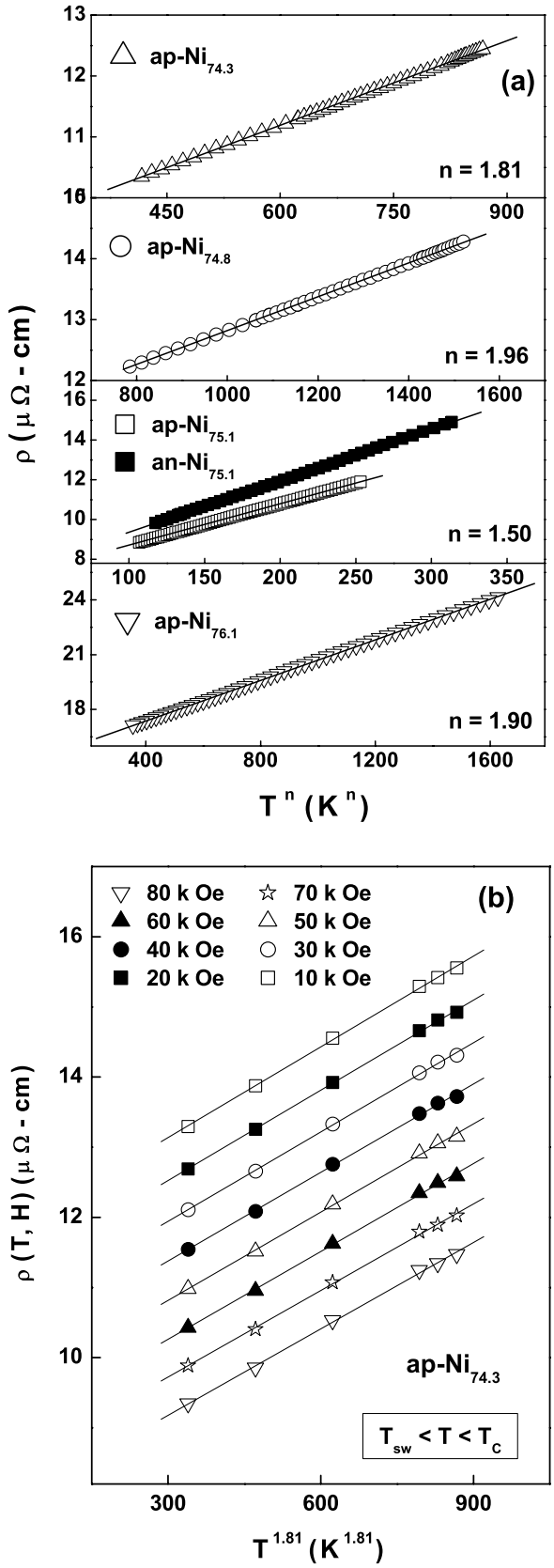

Figure 9. (a) T^n power law variation of resistivity with temperature in the intermediate temperature range. (b) $T^{1.8}$ power law variation of $\rho(T, H)$ for the sample ap-$Ni_{74.3}$ at fixed fields at intermediate temperatures. For the sake of clarity, a constant upward shift of 0.5 $\mu\Omega$ cm has been given to the successive $\rho(T, H)$ data starting from that taken at $H = 80$ kOe.

and experiment. The typical theoretical fits (continuous curves), based on equation (3) and shown in figure 8(a), accurately reproduce the experimentally observed (symbols) field variations of MR within the temperature ranges specified in table 2. The coefficients of various terms have the same values as those predicted by equation (3) but the prefactor 0.304 is exactly one order of magnitude less ($\cong$0.031), with the result that equation (3) predicts MR values that are nearly 10 times the observed ones.

3.2. Intermediate temperatures ($T < T_C$)

In the (intermediate) temperature range that partly overlaps the spin-wave region but falls well below T_C, the spin fluctuation (SF) scattering contribution to $\rho(T)$ and MR becomes more important than that arising from the SW scattering as the thermally excited exchange-enhanced longitudinal and transverse spin-density fluctuations dominate over spin waves. At these temperatures, the theory [8] predicts a *quadratic*

Table 3. Temperature ranges and parameter values corresponding to the fits in the intermediate temperature (spin-density fluctuation) region, based on the relation $\rho(T) = \rho(0) + A_n(0)T^n$ and equation (8) of the text.

Sample label	Temperature range (K)	$\rho(0)$ ($\mu\Omega$ cm)	n	$A_n(0)$ (nΩ cm K^{-n})	$A_n^*(0)$ (nΩ cm K^{-n})	a_λ (10^{-4} Oe$^{-\lambda}$)	λ
ap-$Ni_{74.3}$	28–42 (0.59 T_C–0.88 T_C)	8.30(3)	1.81(1)	4.65(5)	4.70(2)	3.9(1)	0.47(3)
ap-$Ni_{74.8}$	30–42 (0.5 T_C–0.71 T_C)	10.0(1)	1.96(1)	2.71(4)	2.73(4)	1.57(4)	0.60(2)
ap-$Ni_{75.1}$	22–40 (0.4 T_C–0.72 T_C)	6.65(5)	1.50(1)	20.7(2)	21.0(5)	1.81(2)	0.61(1)
an-$Ni_{75.1}$	24–46 (0.45 T_C–0.8 T_C)	6.82(4)	1.50(1)	25.7(3)	25.6(7)	1.75(2)	0.60(1)
ap-$Ni_{76.1}$	22–48 (0.31 T_C–0.68 T_C)	15.2(2)	1.90(1)	5.70(5)	5.69(2)	0.91(1)	0.66(1)

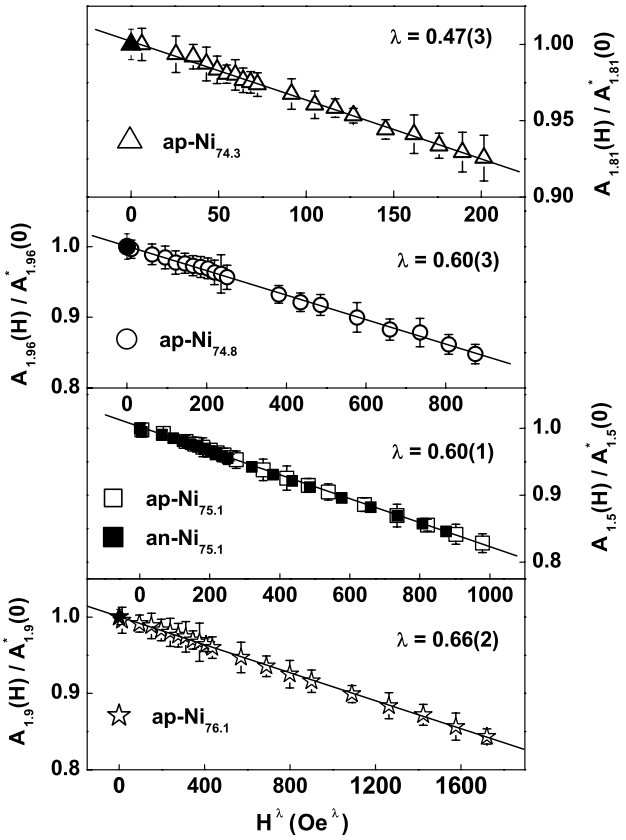

Figure 10. H^λ power law field dependence of the normalized coefficient, $A_n(H)/A_n^*(0)$, of the T^n term in the expression of resistivity at intermediate temperatures.

temperature dependence (i.e. $n = 2$) for both $\rho(T)$ and MR, as in the spin-wave region, but with a totally different value for the coefficient $A_n(0)$ (cf equations (1) and (4)) and for the suppression of the SF contribution, and hence for the variation of MR with field (cf equations (3) and (5)). A comparison of figures 5(a) and 9(a) reveals that the exponent n in $\rho(T) \sim T^n$ increases (decreases) from $n = 1.50(1)$ and 1.66(1) ($n = 1.64(3)$, 1.80(5) and 2.00(2)) to $n = 1.81(1)$ and 1.96(1) ($n = 1.50(1)$, 1.50(1) and 1.90(1)) for ap-$Ni_{74.3}$ and ap-$Ni_{74.8}$ (ap-$Ni_{75.1}$, an-$Ni_{75.1}$ and ap-$Ni_{76.1}$), respectively, as the sample temperature increases from low to intermediate temperatures. Except for the 'as-prepared' (ap) and 'annealed' (an) samples of $Ni_{75.1}$, all the samples (i.e. ap-$Ni_{74.3}$, ap-$Ni_{74.8}$ and ap-$Ni_{76.1}$) have exponent values that do not differ appreciably from the theoretical value, $n = 2$. Another remarkable observation is that the *site disorder* in ap-$Ni_{75.1}$ has *no discernible influence* on the exponent value (1.50(1)). At this stage, it is not clear as to why, in the case of the stoichiometric composition alone, (i) a serious discrepancy exists between the predicted and observed values of n and (ii) the exponent n is insensitive to site disorder. Like in the spin-wave region, at intermediate temperatures, the field H does not affect the temperature variation of resistivity (as illustrated by figure 9(b)), the empirical relation, equation (6), is obeyed (figure 10) with the values of $A_n^*(0)$, a_λ and the exponent λ given in table 3, and $A_n(0) \cong A_n^*(0)$ within the uncertainty limits (see table 3).

In order to ascertain whether or not equation (4) describes correctly the functional dependence of $\Delta\rho_\parallel/\rho$ on H at a given T in the intermediate temperature range, which depends on the composition (table 3), we have adopted the following approach. In accordance with the magnetic equation of state (MES), $[M(T, H)]^2$ versus $H/M(T, H)$ (Arrott) plots at different but fixed values of temperature are constructed out of the magnetization versus field, M–H, isotherms measured on the same samples as those used in the present work. The high-field linear portions of the Arrott plot isotherms (having slope b) are extrapolated to $H = 0$ to yield the values of spontaneous magnetization, M_0, at different temperatures, from the intercepts on the ordinate axis. Inserting the values for the quantities M_0, $[b(3M^2 - M_0^2)]^{-1/2}$, $b(M^2 - M_0^2)$ and $b^2(M^2 - M_0^2)^2$, obtained from Arrott plots and MES, in equation (5) and varying the coefficients of various terms (i.e. basically just two parameters q_0 and c) in equation (5) so as to minimize the least-squares deviations from the measured $(\Delta\rho_\parallel/\rho) - H$ isotherms, we arrive at the theoretical fits (continuous curves) to the $(\Delta\rho_\parallel/\rho) - H$ data (symbols) for different compositions at $T = 0.5T_C$ shown in figure 8(b). Like in the spin-wave region, a perfect agreement between the theoretically predicted [8], equation (5), and experimentally observed variations of MR with field exists at intermediate temperatures (in the ranges specified in table 3) as well, but equation (4) predicts one order of magnitude higher values for MR. We have also verified whether or not equation (5) forms a

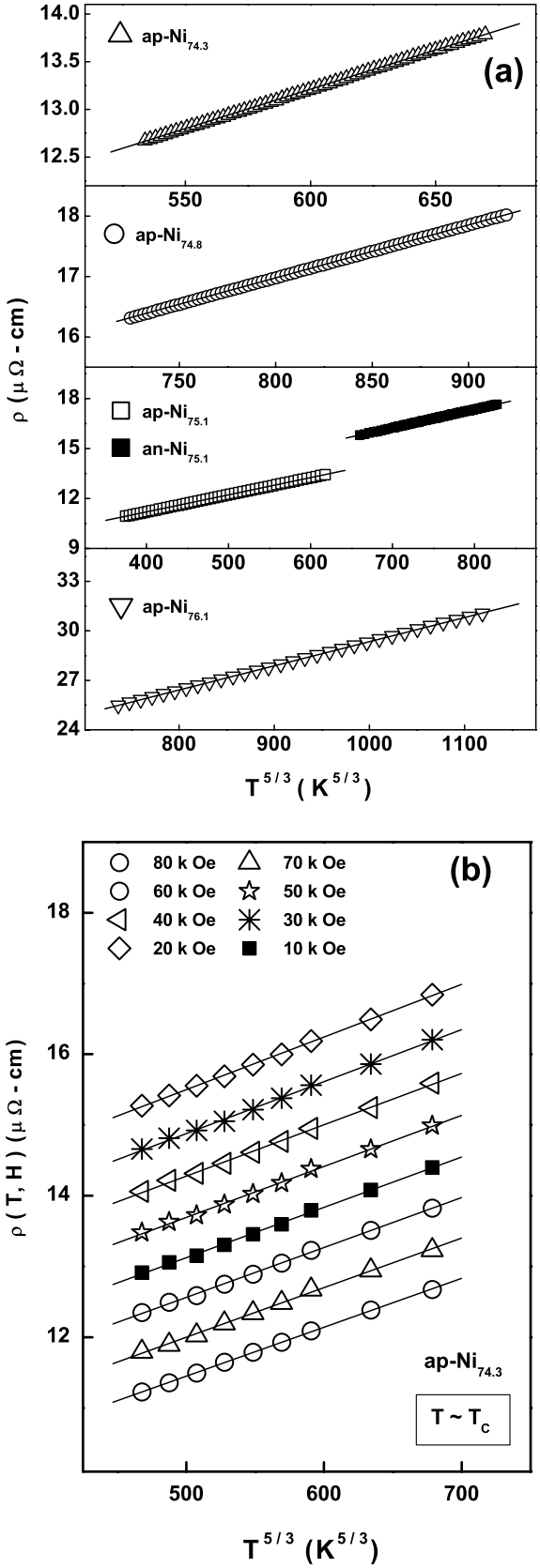

Figure 11. (a) $T^{5/3}$ power law variation of resistivity for temperatures close to the Curie temperature. (b) $T^{5/3}$ power law variation of $\rho(T, H)$ for the sample ap-$Ni_{74.3}$ at fixed fields at temperatures close to the Curie point. For the sake of clarity, a constant upward shift of 0.5 $\mu\Omega$ cm has been given to the successive $\rho(T, H)$ data starting from that taken at $H = 80$ kOe.

unique description of MR(H) at intermediate temperatures by fitting the spin-wave expression, equation (3), (equation (5)) to the MR(H) data in the intermediate (low) temperature region, with the result that equations (3) and (5) are indeed obeyed at low and intermediate temperatures only. This observation thus confirms that spin-wave excitations and non-propagating spin-density fluctuations make dominant contributions at low and intermediate temperatures, respectively.

3.3. Temperatures close to T_C

Consistent with the predictions (equation (6)) of spin fluctuation theory [8], the observed temperature variation of resistivity for all the samples is closely reproduced by the expression $\rho(T) \equiv \rho(T, H = 0) = \rho(0, H = 0) + A_{5/3}(H = 0)T^{5/3}$ at temperatures close to T_C ($0.7T_C \leqslant T \leqslant T_C$), as is evident from figure 11(a). In this temperature range, the scattering of conduction electrons from the longitudinal and transverse non-propagating spin-density fluctuations completely accounts for the electrical resistivity. The coefficient $A_{5/3}(0) \equiv A_{5/3}(H = 0)$ is a direct measure of this spin fluctuation (SF) contribution to resistivity. The composition dependence of $A_{5/3}(0)$, displayed in the top panel of figure 12, depicts the growth of the SF scattering with increasing Ni concentration. As T_C increases with Ni concentration, spin fluctuation modes of larger and larger q (higher energy) get thermally excited for temperatures close to T_C and contribute to resistivity.

As in the case of low and intermediate temperatures, (i) the theoretical result [8] that the field H leaves the temperature variation of resistivity *unaltered* is validated by the behaviour of 'in-field' resistivity, $\rho(T, H)$, observed (figure 11(b)) at temperatures close to T_C, (ii) the empirical relation, equation (8), holds at these temperatures with the values of $A^*_{5/3}(0)$, a_λ and the exponent λ given in table 4 and (iii) $A_{5/3}(0) \cong A^*_{5/3}(0)$ within the error bars (see table 4). The quantities a_λ and λ are plotted as functions of Ni concentration, x, in figure 12 so as to highlight the increasing (decreasing) trend of a_λ (λ) with x. The finding that, at $T \approx T_C$, $\rho(T, H)$ follows the *same* power law ($T^{5/3}$) for *all the compositions* enables us to put equation (8) into the scaling form

$$[A_{5/3}(H)/A_{5/3}(0)] = 1 - (H/H_0)^\lambda \qquad (9)$$

in which H_0 denotes the *critical field* at which the spin-density fluctuations get completely quenched. An extremely good collapse of the $A_{5/3}(H)/A_{5/3}(0)$ versus $(H/H_0)^\lambda$ data for all the compositions onto a single universal curve, demonstrated in figure 13, testifies to the validity of the scaling relation, equation (9). This type of scaling could not be attempted at low and intermediate temperatures because the exponent n depends on composition in those temperature ranges. Consistent with the above inference (drawn based on the $A_{5/3}(0)$ versus x plot shown in figure 12) that higher-energy spin fluctuation modes contribute to resistivity as x increases because higher fields are required to quench high-frequency spin fluctuations, H_0,

Table 4. Temperature ranges and the parameter values corresponding to the fits at temperatures close to the Curie point (spin-density fluctuation region), based on the relation $\rho(T) = \rho(0) + A_n(0)T^n$ and equation (8) of the text.

Sample label	Temperature range (K)	$\rho(0)$ ($\mu\Omega$ cm)	n	$A_n(0)$ (nΩ cm K^{-n})	$A_n^*(0)$ (nΩ cm K^{-n})	a_λ (10^{-4} Oe$^{-\lambda}$)	λ
ap-Ni$_{74.3}$	43.3–49.6 (0.91 T_C–1.04 T_C)	8.27(2)	1.66(1)	8.24(2)	8.25(2)	8.6(1)	0.45(1)
ap-Ni$_{74.8}$	52–60 (0.89 T_C–1.01 T_C)	9.96(7)	1.66(1)	8.77(7)	8.81(4)	11(1)	0.43(1)
ap-Ni$_{75.1}$	36–51 (0.65 T_C–0.92 T_C)	7.09(6)	1.66(3)	10.4(4)	10.4(1)	12(1)	0.42(2)
an-Ni$_{75.1}$	45–56 (0.80 T_C–1.00 T_C)	8.1(1)	1.66(3)	11.5(4)	11.48(5)	14(1)	0.41(1)
ap-Ni$_{76.1}$	47–65 (0.67 T_C–0.93 T_C)	14.8(6)	1.66(2)	15.2(5)	15.2(2)	15.9(6)	0.40(1)

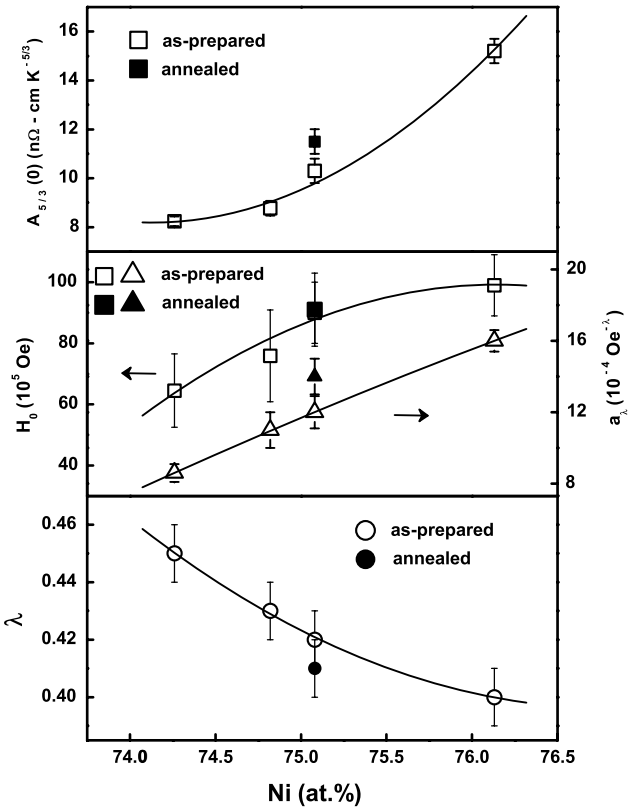

Figure 12. Variations with Ni concentration of the coefficient of the $T^{5/3}$ term in the expression for resistivity, $A_{5/3}(0)$, the exponent λ and the coefficient a_λ of the magnetic field-dependent term in equation (8) as well as of the critical field H_0 in equation (9) at temperatures close to the Curie point.

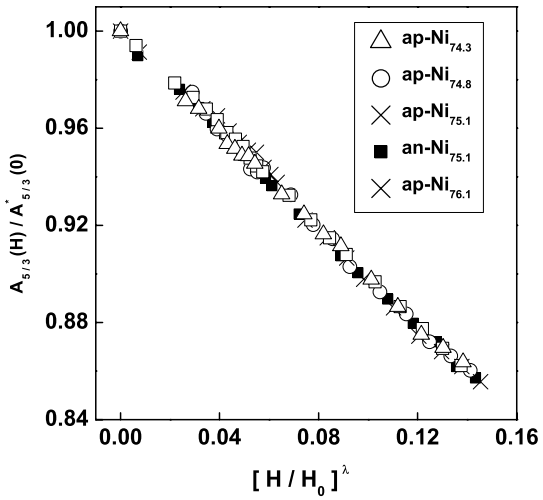

Figure 13. Scaling of the normalized coefficient, $A_{5/3}(H)/A^*_{5/3}(0)$, of the $T^{5/3}$ term in the expression of resistivity with $(H/H_0)^\lambda$ at temperatures close to the Curie point (T_C), in accordance with equation (9) of the text. In this scaling plot, H_0 is the critical field strength required to completely quench the spin-density fluctuations for $T \approx T_C$.

calculated using the relation $H_0 = a_\lambda^{-1/\lambda}$, increases (figure 12) with the Ni concentration, x.

To make a quantitative comparison between the observed and calculated [8] (based on equation (7)) variations of MR with H at fixed temperatures in the vicinity of T_C, the same procedure as that detailed in the previous subsection is followed to arrive at the values for the quantities M_0^2, M_0^4, $[b(3M^2 - M_0^2)]$, $[b(3M^2 - M_0^2)]^2$, $b(M^2 - M_0^2)$ and $b^2(M^2 - M_0^2)^2$ appearing in equation (7) and their coefficients (i.e. just two parameters α and β; the expressions for α and β are given in [8]). The data presented in figure 8(c) clearly demonstrate that the self-consistent theoretical calculations [8] accurately reproduce (continuous curves, based on equation (7)) the observed variations (symbols) of MR with field at temperatures close to T_C but overestimate MR by a factor of 5, as was the case at low and intermediate temperatures as well. Yet another important observation made in this work is that the $(\Delta\rho_\parallel/\rho)$ versus H isotherms at $T = T_C$ (the *critical isotherms*) for all the samples have the unique feature that $(\Delta\rho_\parallel/\rho) \sim H^{0.66}$ (figure 14). This power law behaviour can be understood as follows in terms of the theory, due to Balberg [22], which takes into account the critical fluctuations of the order parameter (spontaneous magnetization) and yields the expression

$$(\Delta\rho_\parallel/\rho) \sim h^{(1-\alpha)/\beta\delta} \tag{10}$$

for the field dependence of magnetoresistance in the critical region ($T \cong T_C$) for a ferromagnet. In equation (8), $h = g\mu_B H/k_B T$ is the reduced field, and α, β and δ are the critical exponents for the 'zero-field' specific heat, spontaneous

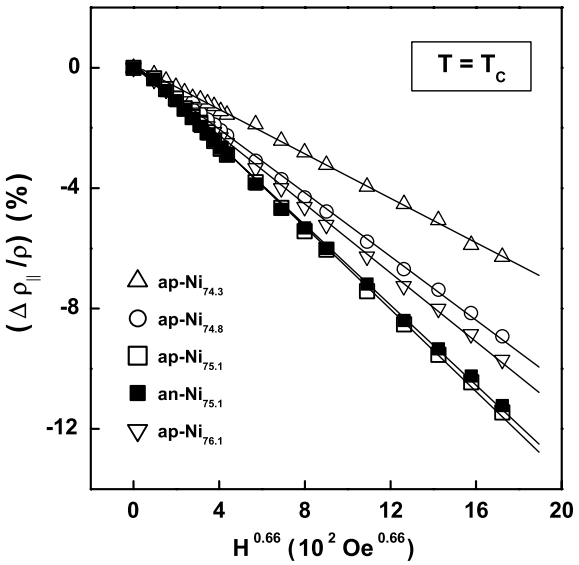

Figure 14. $H^{0.66}$ power law field dependence of the longitudinal magnetoresistance, $\Delta\rho_{\parallel}/\rho$, at $T = T_C$.

magnetization and the M versus H isotherm at $T = T_C$, respectively. An extensive study of critical phenomena in ap-$Ni_{74.3}$, ap-$Ni_{74.8}$, ap-$Ni_{75.1}$, an-$Ni_{75.1}$ and ap-$Ni_{76.1}$ samples have yielded [16, 23, 24] *mean-field* values for the critical exponents β, γ (the critical exponent for initial susceptibility) and δ, i.e. $\beta = 0.500(3)$, $\gamma = 1.000(5)$ and $\delta = 3.000(4)$. Inserting these values for the exponents β and γ in the Rushbrooke equality $\alpha + 2\beta + \gamma = 2$, yields $\alpha = 0$. With $\alpha = 0$, $\beta = 0.5$ and $\delta = 3.0$, equation (10) reduces to exactly the same form, $(\Delta\rho_{\parallel}/\rho) \sim h^{2/3}$, as that observed in this work. Interestingly, equation (7) provides as good a quantitative description of the critical $(\Delta\rho_{\parallel}/\rho)$ versus H isotherms for all the compositions as equation (10) does. This is because the theoretical formalism [8] leading to equation (7) makes use of the mean-field equation of state, which is consistent with the above values for the critical exponents.

Finally, the composition dependence of negative MR at $T/T_C = 0.2$, 0.5 and 0.9 (that fall within the low, intermediate and near T_C temperature regions, respectively) is highlighted by the insets in figure 8. These insets demonstrate that: (i) at any fixed value of H (shown only for $H = 8$ T but true for other fields as well), the *negative* MR goes through a *peak* at the stoichiometric composition at all temperatures and (ii) regardless of composition, the negative MR increases as the temperature is progressively raised from low temperatures so as to approach T_C from below. These observations imply that, irrespective of the temperature range (low, intermediate or close to T_C), the maximum suppression of the dominant magnetic excitation by magnetic field occurs for the stoichiometric composition, and that the amplitude of the thermally excited spin fluctuation modes picks up rapidly as T_C is approached, with the result that, at any field strength, the suppression is maximum at T_C.

4. Summary and conclusions

Extensive high-resolution electrical resistivity, $\rho(T)$, and longitudinal magnetoresistance, $\Delta\rho_{\parallel}/\rho = [\rho_{\parallel}(T, H) - \rho(T, H = 0)]/\rho(T, H = 0)$, measurements have been carried out on well-characterized 'as-prepared' Ni_xAl_{100-x} alloys with $x = 74.3$, 74.8, 75.1 and 76.1 at.% and on the 'annealed' $Ni_{75.1}Al_{24.9}$ alloy at temperatures in the range $1.7\ \text{K} \leqslant T \leqslant 300\ \text{K}$ and in magnetic fields, H, up to 80 kOe. At low temperatures in the range $1.7\ \text{K} \leqslant T < 25\ \text{K}$, electrical resistivity exhibits *non-Fermi liquid* (NFL) behaviour in the samples ap-$Ni_{74.3}$, ap-$Ni_{74.8}$, ap-$Ni_{75.1}$ and an-$Ni_{75.1}$. In contrast, $\rho(T)$ in ap-$Ni_{76.1}$ follows the T^2 law (the Fermi liquid behaviour) over a narrow temperature range $1.7\ \text{K} \leqslant T \leqslant 16\ \text{K}$. As the critical concentration, $x_c \cong 73.6$ at.%, is approached from above, i.e. as the *compositional disorder* increases, *stronger deviations* from the Fermi liquid behaviour occur and the temperature range over which the NFL *behaviour* persists *widens*. By contrast, the *site disorder* makes the NFL behaviour *more prominent*, particularly in the *stoichiometric* composition (Ni_3Al), and stabilizes the NFL behaviour in any given composition over a *much wider* temperature range. Based on plausible arguments, it is proposed that the NFL behaviour observed at low temperatures when x falls below 76.1 at.% reflects that the increased compositional disorder *alters the spin-wave dispersion* at *finite* q such that, as q increases from $q = 0$, the spin-wave dispersion becomes increasingly similar to the non-propagating spin fluctuation dispersion prevalent at temperatures close to T_C (Curie temperature).

The expression $\rho(T, H) = \rho(0, H) + A_n(H)T^n$ with $H = 0$ and $H \neq 0$ forms an excellent description of the 'zero-field', $\rho(T, H = 0)$, and 'in-field', $\rho(T, H)$, resistivities at all temperatures below T_C. The values of the quantities $\rho(0) \equiv \rho(0, H = 0)$, $\rho(0, H)$, $A_n(0)$, $A_n(H)$ and the exponent n *depend on* the sample composition and on the choice of the temperature range but in any given temperature range, n is *independent* of H. The observation that the exponent n does not depend on H vindicates the theoretical approach [8], recently proposed by one of the authors. The functional dependence of A_n on H is accurately described by the empirical relation $A_n(H) = A_n(0)[1 - a_\lambda H^\lambda]$ over the entire temperature range $T \leqslant T_C$ but with the coefficient a_λ and the exponent λ varying from sample to sample and from one temperature regime to the other. For temperatures close to T_C, where, in accordance with the theoretical predictions [8], the exponent n has the *universal* value of $n = 5/3$, the $A_n(H)$ data for all the samples collapse onto the *universal plot* of $A_{5/3}(H)/A_{5/3}(0)$ versus $(H/H_0)^\lambda$. The critical field, H_0, required to completely quench the spin-density fluctuations increases with the Ni concentration, x.

Contrasted with the above empirical relation, which quantifies the suppression of the dominant magnetic excitations at a *given field strength over a specified temperature range* (low temperatures or intermediate temperatures or temperatures close to T_C), the self-consistent theoretical treatment [8] calculates the suppression of such excitations with *varying*

magnetic field at a fixed temperature in a particular temperature range. A quantitative comparison between the theoretical predictions [8] and the $(\Delta\rho_{\parallel}/\rho) - H$ isotherms taken in different temperature regimes, which makes use of the magnetization, $M(T, H)$, data taken on the same samples as the present ones at temperatures 5 K $\leqslant T \leqslant$ 300 K and magnetic fields 0 kOe $\leqslant H \leqslant$ 70 kOe, reveals that the self-consistent spin fluctuation theory [8] predicts correctly the observed variations of $\Delta\rho_{\parallel}/\rho$ with H at low temperatures, intermediate temperatures and temperatures close to, or even equal to, T_C. The $(\Delta\rho_{\parallel}/\rho)$ versus H isotherms taken at $T = T_C$ (the *critical isotherms*) for all the samples have the *common feature* that $(\Delta\rho_{\parallel}/\rho) \sim H^{2/3}$. The theory, due to Balberg [22], is shown to provide a straightforward explanation for the observed power law behaviour.

Other important observations that deserve a mention are: (i) at any fixed value of H, the *negative* magnetoresistance (MR) goes through a *peak* at the stoichiometric composition at all temperatures and (ii) regardless of composition, the negative MR increases as the temperature increases from low temperatures to $T = T_C$. These observations imply that, irrespective of the temperature range (low, intermediate or close to T_C), the maximum suppression of the dominant magnetic excitation by magnetic field occurs for the stoichiometric composition, and that the amplitude of the thermally excited spin fluctuation modes picks up rapidly as T_C is approached, with the result that, at any field strength, the suppression is maximum at T_C.

Acknowledgments

This work was supported by the Department of Science and Technology, India, under grants SP/S2/M-21/97 and SP/I2/MF-02-96-D. One of the authors (ACA) is grateful to the Council of Scientific and Industrial Research, India, for financial support.

References

[1] Mills D L and Lederer P 1966 *J. Phys. Chem. Solids* **27** 1805
[2] Schindler A I and Rice M J 1967 *Phys. Rev.* **164** 759
[3] Mathon J 1968 *Proc. R. Soc.* A **306** 355
[4] Ueda K and Moriya T 1975 *J. Phys. Soc. Japan* **39** 605
[5] Moriya T and Kawabata A 1973 *J. Phys. Soc. Japan* **34** 639
Moriya T and Kawabata A 1973 *J. Phys. Soc. Japan* **34** 669
[6] Ueda K 1976 *Solid State Commun.* **19** 965
[7] Pai R V and Mishra S G 1993 *Phys. Rev.* B **48** 10292
[8] Kaul S N 2005 *J. Phys.: Condens. Matter* **17** 5595
[9] Moriya T 1985 *Spin Fluctuations in Itinerant Electron Magnetism* (*Springer Series in Solid State Sciences* vol 56) (Berlin: Springer)
[10] Fluitman J H J, Boom R, De Chatel P F, Schinkel C J, Tilanus J L L and De Vries B R 1973 *J. Phys. F: Met. Phys.* **3** 109
[11] Chang K H, van der Linde R H and Sieverts E G 1973 *Physica* **69** 467
[12] Hambourger P D, Olwert R J and Chu C W 1975 *Phys. Rev.* B **11** 3501
[13] Sasakura H, Suzuki K and Masuda Y 1984 *J. Phys. Soc. Japan* **53** 352
[14] Yoshizawa M, Seki H, Ikeda K, Okuno K, Saito M and Shigematsu K 1992 *J. Phys. Soc. Japan* **61** 3313
[15] Fuller C J, Lin C L, Mihalisin T, Chu F and Bykovetz N 1992 *Solid State Commun.* **83** 863
[16] Semwal A and Kaul S N 2002 *J. Phys.: Condens. Matter* **14** 5829
Rhee J Y, Kudryavtsev Y V and Lee Y P 2003 *Phys. Rev.* B **68** 045104
[17] Aoki K and Izumi O 1975 *Phys. Status Solidi* **32** 657
[18] Semwal A and Kaul S N 1999 *Phys. Rev.* B **60** 12799
[19] Kaul S N 1999 *J. Phys.: Condens. Matter* **11** 7597
[20] Steiner M J, Beckers F, Nilkowitz P G and Lonzarich G G 2003 *Physica* B **329–333** 1079
[21] Milkowitz P G, Beckers F, Lonzarich G G, Kneble G, Salce B, Thomsson J, Bernhoeft N, Braithwaite D and Flouquet F 2005 *Phys. Rev.* B **72** 024424
[22] Balberg I 1977 *Physica* B **91** 71
[23] Semwal A and Kaul S N 2001 *Phys. Rev.* B **64** 014417
[24] Abhyankar A C, Semwal A and Kaul S N 2008 *J. Phys.: Condens. Matter* **20** 445228